

# Hierarchical Structure and Nanomechanics of Collagen Microfibrils from the Atomistic Scale Up

Alfonso Gautieri,<sup>†,‡</sup> Simone Vesentini,<sup>‡</sup> Alberto Redaelli,<sup>‡</sup> and Markus J. Buehler<sup>\*,†,§,||</sup>

<sup>†</sup>Laboratory for Atomistic and Molecular Mechanics, Department of Civil and Environmental Engineering, Massachusetts Institute of Technology, 77 Massachusetts Avenue Room 1-235A&B, Cambridge, Massachusetts 02139, United States

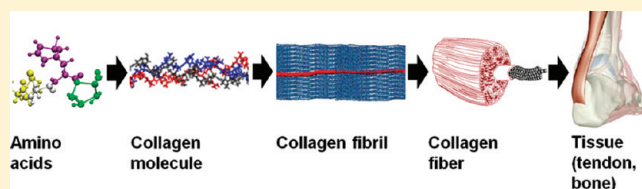
<sup>‡</sup>Department of Bioengineering, Politecnico di Milano, P.zza Leonardo da Vinci 32, 20133, Milano, Italy

<sup>§</sup>Center for Materials Science and Engineering, <sup>||</sup>Center for Computational Engineering, Massachusetts Institute of Technology, 77 Massachusetts Avenue, Cambridge, Massachusetts 02139, United States

**ABSTRACT:** Collagen constitutes one-third of the human proteome, providing mechanical stability, elasticity, and strength to organisms and is the prime construction material in biology. Collagen is also the dominating material in the extracellular matrix and its stiffness controls cell differentiation, growth, and pathology. However, the origin of the unique mechanical properties of collagenous tissues, and in particular

its stiffness, extensibility, and nonlinear mechanical response at large deformation, remains unknown. By using X-ray diffraction data of a collagen fibril (Orgel, J. P. R. O. et al. *Proc. Natl. Acad. Sci.* **2006**, *103*, 9001) here we present an experimentally validated model of the nanomechanics of a collagen microfibril that incorporates the full biochemical details of the amino acid sequence of constituting molecules and the nanoscale molecular arrangement. We demonstrate by direct mechanical testing that hydrated (wet) collagen microfibrils feature a Young's modulus of  $\approx 300$  MPa at small, and  $\approx 1.2$  GPa at larger deformation in excess of 10% strain, which is in excellent agreement with experimental data. We find that dehydrated (dry) collagen microfibrils show a significantly increased Young's modulus of  $\approx 1.8$ – $2.25$  GPa, which is in agreement with experimental measurements and owing to tighter molecular packing. Our results show that the unique mechanical properties of collagen microfibrils arise due to their hierarchical structure at the nanoscale, where key deformation mechanisms are straightening of twisted triple-helical molecules at small strains, followed by axial stretching and eventual molecular uncoiling. The establishment of a model of hierarchical deformation mechanisms explains the striking difference of the elastic modulus of collagen fibrils compared with single molecules, which is found in the range of  $4.8 \pm 2$  GPa, or  $\approx 10$ – $20$  times greater. We find that collagen molecules alone are not capable of providing the broad range of mechanical functionality required for physiological function of collagenous tissues. Rather, the existence of an array of deformation mechanisms, derived from the hierarchical makeup of the material, is critical to the material's ability to confer key mechanical properties, specifically large extensibility, strain hardening, and toughness, despite the limitation that collagenous materials are constructed from only few distinct amino acids. The atomistic model of collagen microfibril mechanics now enables the bottom-up elucidation of structure–property relationships in a broader class of collagen materials (e.g., tendon, bone, cornea), including studies of genetic disease where the incorporation of biochemical details is essential. The availability of a molecular-based model of collagen tissues may eventually result in novel nanomedicine approaches to develop treatments for a broad class of collagen diseases and the design of de novo biomaterials for regenerative medicine.

**KEYWORDS:** Collagen, mechanical properties, deformation, molecular simulation, nanomechanics, materiomics



Collagen molecules represent the most abundant construction material in the human body, where they provide mechanical stability, elasticity, and strength to connective tissues such as tendons, ligaments, and bone, as well as the extracellular matrix (ECM).<sup>1–3</sup> Yet, we understand relatively little about how collagen molecules combine to form larger-scale structural elements such as fibrils and fibers and how they provide crucial mechanical properties to organisms. It is known that virtually all collagen-based tissues are organized into hierarchical structures, where the lowest hierarchical level consists of triple helical collagen molecules (Figure 1).<sup>2–9</sup> Collagen fibrils consist of high-aspect-ratio polypeptides, tropocollagen molecules, with a

length of  $\approx 300$  nm and a diameter of about 1.5 nm, which are arranged in a staggered configuration. This structure creates an observable periodicity known as the *D*-band, where  $D = 67$  nm. The collagen molecule's length is not a multiple of *D*, where in terms of *D* the collagen molecule measures  $4.46 D$ . According to the Hodge–Petruska model,<sup>10</sup> a structural model of collagen fibrils, molecules in a fibril are deposited side by side and parallel but staggered with respect to each other, where the molecular

**Received:** November 10, 2010

**Revised:** December 7, 2010

**Published:** January 5, 2011

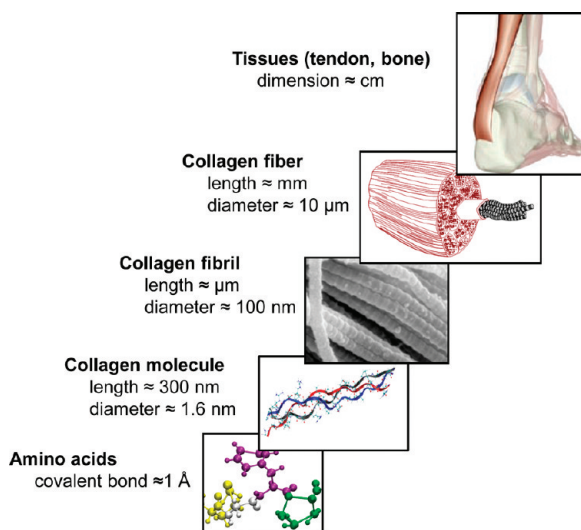


**Figure 1.** Hierarchical structure of collagen protein materials.<sup>1–9</sup> Each collagen molecule is made of three peptide chains that form the  $\approx 300$  nm long triple helical collagen molecule. Collections of collagen molecules aggregate both in lateral and longitudinal directions to form fibrils. Fibrils in cornea are normally thin ( $\approx 30$  nm) and uniform in diameter, while tissues such as tendon contain a wide-ranging distribution of diameters (100–500 nm). Fibrils include tiny hydroxyapatite crystals in bone tissue, which provide stiffness and compressive load resistance. In tendons and ligaments, multiple fibrils make up collagen fiber, formed with the aid of proteoglycans.

axes are parallel to the fibril direction. A gap between two consecutive collagen molecules is known as the “gap region” and measures  $0.54 D$ , or  $\approx 36$  nm.<sup>10</sup> Collagen fibrils have a diameter of 100–500 nm and a length up to the millimeter range and are formed through the bundling of several microfibrils that each contain clusters of five collagen molecules.<sup>11</sup> At the next level of the hierarchy, multiple fibrils make up the collagen fiber, formed with the aid of cross-linking macromolecules such as proteoglycans. In bone, the organic collagen protein matrix is stiffened via the inclusion of mineral hydroxyapatite crystals that emerge from the gap regions.<sup>3,7,12,13</sup>

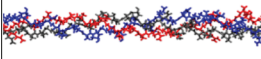
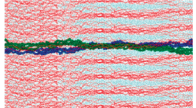
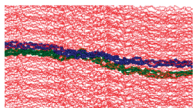
To determine how collagen-based structures confer mechanical properties to tissues like skin, tendon, and bone and to identify how cells interact with the ECM, the understanding of the mechanics at different hierarchical levels and their interplay from a biochemical and molecular level upward is essential. Earlier work has demonstrated that mechanical strain is distributed over distinct hierarchical levels (molecules, fibrils, fibers)<sup>14–16</sup> and that collagen tissue stretching involves concurrent deformation mechanisms, where the measured stiffnesses of the tissue at different scales varies vastly. Significant efforts have been made in recent years focused on characterizing the mechanical properties of collagen by using experimental, computational, and theoretical approaches. A review of recent works aimed at the understanding of the structure and mechanical properties of collagen-based tissues is nicely summarized in recent contributions.<sup>3,17</sup> Earlier work was mostly focused on the macroscopic, overall mechanical properties of collagen fibers and related tissues with several efforts that elucidated the mechanics of hierarchical structures.<sup>3,12,14,18–21</sup> Other studies focused solely on the properties of individual tropocollagen molecules without linking to the larger scale materials response.<sup>22–25</sup> Most recently, experimental reports focused on the mechanical properties of individual

collagen fibrils, which provided important insight into the Young's modulus and their nonlinear deformation behavior.<sup>26–28</sup> However, most of these studies did not yet incorporate molecular details into their investigations. To the best of the authors' knowledge, exceptions are the pioneering works by Sasaki and Odajima<sup>29</sup> and by Fratzl et al.<sup>30</sup> By applying X-ray diffraction methods these groups investigated the elongation mechanism of tendon collagen on the basis of the hierarchical structure of the tissue and including the arrangement of collagen molecules in the tissue. These authors proposed models to describe how collagen molecules in fibrils are elongated and rearranged due to external force.<sup>30,31</sup>

Molecular modeling provides a powerful approach to complement experimental approaches and to describe the molecular mechanics of collagen from the bottom up and at multiple scales. Most studies, however, were based on ultrashort collagen-like peptides obtained from X-ray crystallography.<sup>32–35</sup> The early molecular simulation studies used these short collagen molecules<sup>36–41</sup> that were typically limited to less than 10 nm length or more than a factor of 30 smaller than actual molecules found in collagen tissues. The resulting elastic modulus of these short collagen peptides was found to be in the range of  $4.8 \pm 2$  GPa and much greater than the typical Young's moduli measured for macro-scale collagen tissues, yet in agreement with single molecule studies<sup>22,23,42–44</sup> (Table 1). The direct study of larger assemblies of collagen molecules into microfibrils and fibers with full atomistic simulation methods has remained elusive due to the lack of an appropriate atomistic description and the size of the system. Some reports of molecular modeling of collagen microfibrils are based on a two-dimensional coarse-grained model, where collagen molecules are described in a mesoscale bead–spring model.<sup>45,46</sup> While the bead–spring model showed key features of the stress–strain behavior found in experiments, a disagreement of the magnitude of the predicted modulus was identified that could not be reconciled. Furthermore, earlier bead–spring models retained little information of the primary sequence, did not include a description of the three-dimensional arrangement of collagen molecules and lacked the ability to deal with explicit water solvent (i.e., a model that includes the simulation of all water molecules based on their atomic structure). These issues are, however, likely important for collagen mechanics and must be incorporated in a rigorous bottom-up tissue mechanics description that links genetics to structure to mechanics. The need of defining the material properties of collagenous tissues from the biochemistry level upward is clearly demonstrated when considering the effect of mutations in collagen, which can result in incorrectly assembled collagen protein that cause a variety of severe and sometimes deadly pathologies, such as Ehlers-Danlos syndrome, scurvy or *osteogenesis imperfecta* (brittle bone disease).<sup>47</sup>

**2. Results and Discussion.** Here we use an atomistic collagen microfibril model that includes full-length molecules with the actual amino acid sequence defined by the human collagen gene and that thus completely captures the biochemical features of collagen molecules to describe the mechanical behavior at the microfibril level (see Materials and Methods for details). To the best of our knowledge, no such modeling of the mechanical properties at this scale has been previously attempted. The basis of our microfibril model is the recently reported structure of native in situ collagen in rat tail tendon.<sup>6,8</sup> By employing crystallographic techniques in X-ray fiber diffraction experiments, Orgel et al.<sup>8</sup> obtained the packing arrangement of collagen molecules in

**Table 1.** Comparison of Young's Modulus of Collagen Molecule (Solvated) and Collagen Microfibril (Including Hydrated [Wet] and Dehydrated [Dry] States) As Predicted from Experimental and Theoretical Analyses<sup>67,68</sup>

Hierarchical level or state	Type of analysis	Young's Modulus (GPa)
Collagen molecule (averaged value 4.8±2.0 GPa) 	X-Ray diffraction <sup>43</sup>	≈3
	Brillouin light scattering <sup>22</sup>	≈5.1
	Brillouin light scattering <sup>44</sup>	≈9
	Estimate based on persistence length <sup>23</sup>	0.35–12
	Estimate based on persistence length <sup>42</sup>	≈3
	Atomistic modeling <sup>37</sup>	≈4.8
	Reactive atomistic modeling <sup>38</sup>	≈7
	Atomistic modeling <sup>67</sup>	≈2.4
	Atomistic modeling <sup>40</sup>	≈4
	Coarse-grain modeling <sup>68</sup>	≈4
Collagen microfibril, wet (averaged value 0.6±0.2 GPa) 	X-ray diffraction <sup>29</sup>	0.43 (small strain)
	AFM testing <sup>27</sup>	0.2–0.8 (small strain)
	MEMS stretching <sup>26, 28</sup>	0.86 ± 0.45 (small strain) 0.72 ± 0.57 (large strain)
	Bead-spring based mesoscale model <sup>45, 46</sup>	4.36 (smaller strain) ≈38 (significantly larger strain)
	Atomistic modeling (present study)	≈0.3 (small strain) ≈1.2 (large strain)
	AFM testing <sup>27</sup>	2–7
Collagen microfibril, dry (averaged value 3.26 GPa) 	Atomistic modeling (present study)	≈1.8 ≈2.25 (larger strain)

a collagen microfibril, resulting in the three-dimensional geometry of collagen molecules including the N- and C-telopeptides. On the basis of the data from X-ray diffraction experiments, however, only the positions of the C $\alpha$  backbone atoms in the collagen microfibril are available, and as a result the model reported in ref 8 did not yet include all atomistic details of the supermolecular assembly in collagen fibrils. To develop a full atomistic representation, we use a computational approach to add all missing atoms including the side chains into the structure and identify the most stable configuration by using the all-atom CHARMM force field and a statistical structure identification approach (see Materials and Methods). Since the backbone structure is known, this homology modeling followed by extensive molecular equilibration provides a reliable estimate of the structure of the side chains.

The resulting atomistic model features full ≈300 nm long collagen molecules including the telopeptide domains attached at the ends of each molecule, and incorporates the complete three-dimensional arrangement of collagen molecules arranged in a periodic unit cell (Figure 2a). The unit cell dimension in the Z-axis corresponds to the length of the characteristic D-period observed for collagen fibrils. Thus, a full length collagen molecule spans five periodic cells in the Z-axis direction. Figure 2b shows the N-terminal portion of the original collagen molecule (in red) with four periodic images represented in gray, illustrating how the unit cell represents a model for the larger-scale molecular assembly into collagen microfibrils. Since the model uses periodic boundary conditions, it resembles infinitely large collagen

microfibrils in each dimension. The staggering of the molecules along the molecular axis leads to the well-known D-banding periodicity (Figure 2c), while the molecules are arranged in a quasi-hexagonal pattern in the orthogonal direction where five molecules form the characteristic microfibril structure (Figure 2d).<sup>8</sup> Within each periodic cell, collagen molecules interdigitate with neighboring molecules to form a supertwisted right-handed microfibril. The characteristic banded structure of the equilibrated atomistic model of the collagen microfibril emerges naturally due to the three-dimensional structure of both single molecules and their assembly in the longitudinal and axial directions, and is found to be stable in our molecular model. Figure 2e illustrates a D-period with five molecular strands that form a collagen microfibril, showing the gap and overlap regions that arise because one of the strands forming the microfibril is shorter than the D-period itself. The obtained D-banding reproduces experimental microscopy images of collagen fibrils well, owing to the fact that our molecular model is based on X-ray diffraction data and stable after molecular equilibration<sup>48</sup> (Figure 3a,b).

We first report an account of the difference of the structural features of a fully equilibrated full-atomistic collagen microfibril in both hydrated (wet) and dehydrated (dry) conditions. In our study, the dehydrated collagen microfibril model is used to assess the effect of hydration on the mechanical properties of collagen fibrils, which has been shown experimentally to be an important factor in defining structure and properties of collagenous tissues. The equilibration of the hydrated collagen microfibril



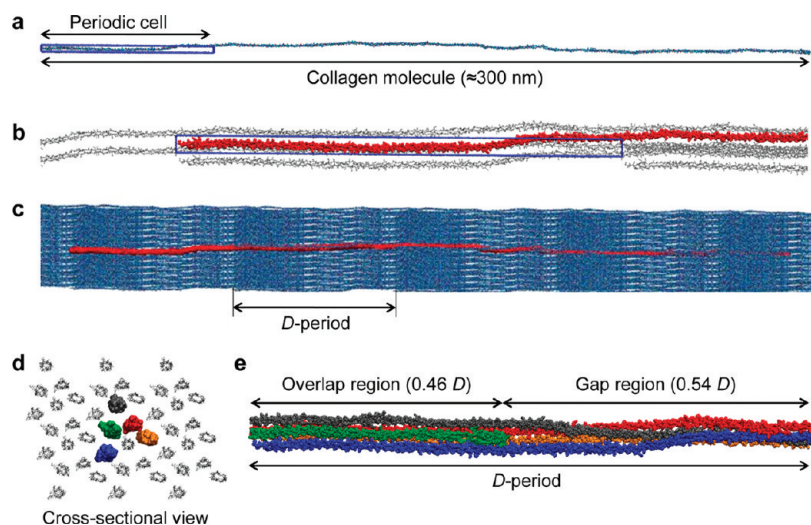


**Figure 2.** Atomistic model of the collagen microfibril. The full-atomistic model of the collagen microfibril is generated starting from the in situ structure of the backbone geometry of full length collagen type I molecule as identified by X-ray diffraction and using the associated information on the naturally occurring crystallographic unit cell ( $a \approx 40.0$  Å,  $b \approx 27.0$  Å,  $c \approx 678$  Å,  $\alpha \approx 89.2^\circ$ ,  $\beta \approx 94.6^\circ$ ,  $\gamma \approx 105.6^\circ$ )<sup>8</sup> (PDB ID 3HR2). Panel a shows that homology modeling is used to obtain the full-atom structure of the human collagen type I molecule. The collagen supramolecular model of the microfibril is generated by the periodic repetition of the unit cell. Panel b shows a portion of the original collagen molecule in red, while four periodic images of the molecule are represented in gray. The molecular packing topology obtained by the periodic repetition of the unit cell leads to the well-known  $D$ -banding periodicity seen in AFM images of collagen microfibrils as shown in panel c (in red the original molecule, in blue the periodic images). Panel d shows the quasi-hexagonal packing of collagen molecules, which interdigitates with neighboring molecules to form a supertwisted right-handed microfibril as depicted in panel e. This image is obtained wrapping all collagen atoms (which spans several periodic units, see panel a) into a unit cell in order to visualize the microfibril periodic unit.

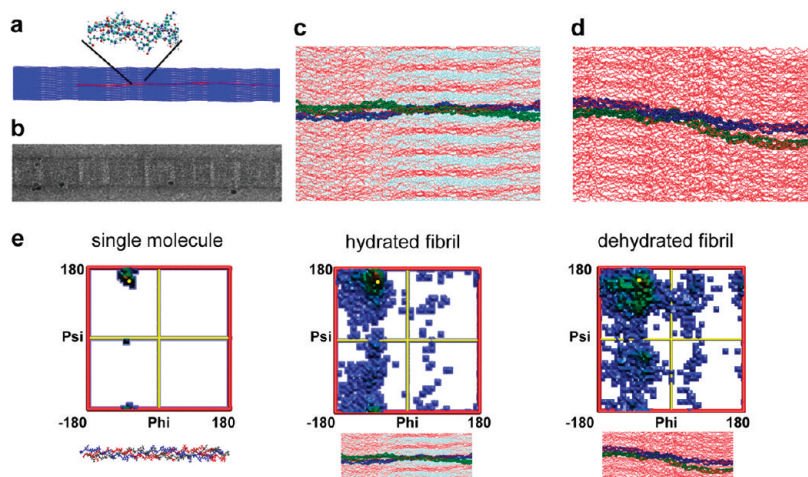


**Figure 3.** Structural analysis and validation of atomistic collagen microfibril models. Comparison of the  $D$ -periodic banding observed for the full-atomistic microfibril model (panel a) and experimentally with SEM techniques (panel b, reprinted with permission from ref 48 (Copyright 2001 National Academy of Sciences, U.S.A.)). Panel c shows a detailed view of the equilibrated structure in proximity of the gap-overlap region, showing collagen molecules (in red, plus two highlighted molecules in blue and green) and water molecules (cyan). Panel d shows a snapshot of the gap-overlap transition region for the equilibrated dehydrated collagen microfibril, which represents a much denser packing of molecules. Ramachandran diagram for a short collagen like peptide (left, panel e) and for the hydrated full atomistic microfibril (center, panel e) and for the dehydrated collagen microfibril (right, panel e), showing that the configuration is close to that of the polyproline II chain ( $\psi \approx 150^\circ$ ,  $\phi \approx -75^\circ$ , yellow dot) and thus close to the expected configuration of a collagen molecule. The dehydrated microfibril shows a more disperse distribution of dihedral angles.

(Figure 3c) leads to a density of  $\approx 1.19$  g/cm<sup>3</sup>, a value that is halfway between the density of water and the density of dehydrated collagen, which has been estimated at 1.34 g/cm<sup>3</sup>.<sup>49</sup> A Ramachandran analysis of the solvated system (Figure 3e, center) shows that the collagen microfibril lies in a region of the diagram ( $\psi \approx 150^\circ$ ,  $\phi \approx -75^\circ$ ) that is characteristic of the polyproline II chain and thus of collagen-like peptides

(Figure 3e, left), in good agreement with experimental structural studies.<sup>50</sup> The density of the dehydrated (dry) collagen microfibril (Figure 3d) reaches a larger density, with a value of  $\approx 1.29$  g/cm<sup>3</sup>. A Ramachandran analysis of the dehydrated collagen microfibril (Figure 3e, right) shows that it also lies in a region of the diagram that is characteristic of collagen-like peptides ( $\psi \approx 150^\circ$ ,  $\phi \approx -75^\circ$ ); however, a broader range of dihedral angles is found

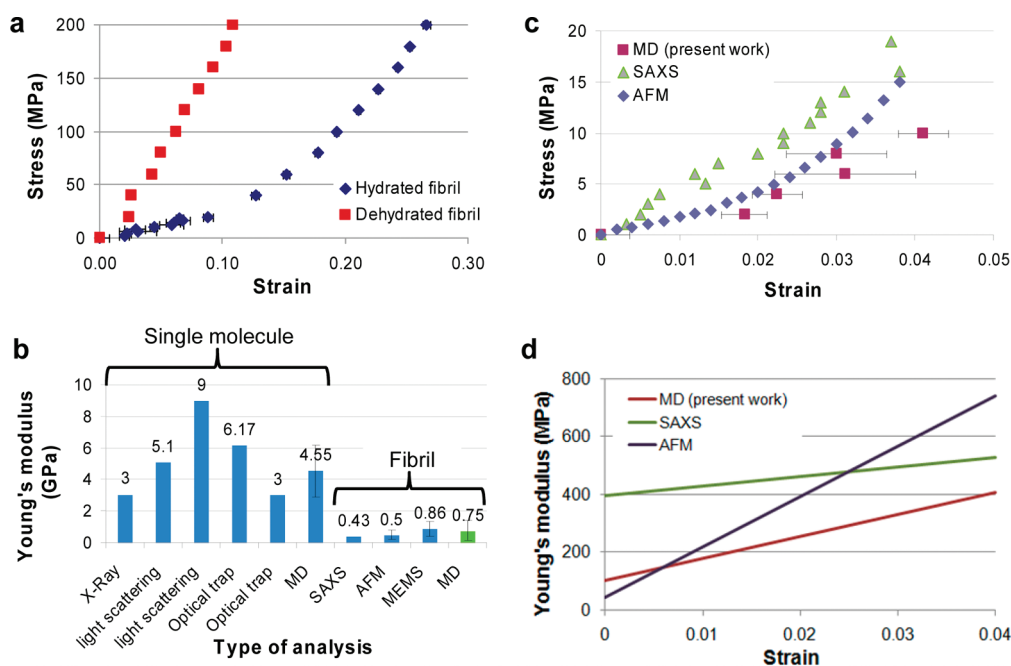


**Figure 4.** Collagen microfibril stress–strain behavior, comparison with single molecule mechanics, and quantitative comparison with experimental results. The mechanical properties of both hydrated and dehydrated collagen microfibrils are determined imposing an increasing mechanical stress (negative pressure) along the fibril axis while maintaining the pressure on the other axes constant at 1 bar. Mechanical testing yields a fibrillar small-strain Young's modulus of  $\approx 300$  MPa and a large-strain modulus of  $\approx 1.2$  GPa for the hydrated model, while an almost linear behavior and an elastic modulus of  $\approx 1.8$  GPa (approaching 2 GPa for larger strains) is found for the dehydrated model (panel a). This finding suggests that the dehydrated collagen microfibril tends to have a greater stiffness, a finding that is in agreement with experimental results (see Table 1). (Panel b) Direct comparison of the Young's modulus obtained for solvated single molecules and microfibrils, featuring various experimental results and the predictions from our microfibril mechanics model. The calculated Young's modulus for the solvated collagen microfibril (green) results in very good agreement with experimental findings based on a variety of techniques including SAXS, AFM, and MEMS testing, which yield a small strain fibril Young's modulus in the range of few hundred megapascals. (Panel c) Direct comparison of stress–strain curves obtained in this work and those obtained with experimental techniques. (Panel d) Young's modulus over strain (obtained from the gradient of stress–strain curves), comparing experiment and simulation for hydrated microfibrils.

indicating some level of molecular unfolding. This suggests that the loss of water results in a loss of structure at the molecular scale, indicating that water is indeed needed to keep the characteristic configuration of collagen molecules in microfibrils. This agrees with earlier work on collagen-like peptides at the single molecule scale where a greater level of disorder and loss of H-bonding was found in vacuum studies.<sup>36</sup> Overall, our model shows good quantitative agreement with available experimental structural data of collagen microfibrils, which confirms that the molecular representation based on X-ray data is a good starting point for the analysis of its mechanical properties.

With this structurally validated collagen microfibril model at hand, we now test the mechanical properties of a hydrated and dehydrated collagen microfibril by applying constant stress boundary conditions along the fibril axis and monitoring the resulting strain at equilibrium. We assess stresses in the range from 0 to 200 MPa, leading to the stress–strain behaviors shown in Figure 4a. We find that hydrated collagen microfibrils feature two distinct deformation regimes. In the small-strain regime (<10%), the predicted Young's modulus is  $\approx 300$  MPa, while in the large-strain regime (>10%) the microfibril shows a severely increased tangent stiffness with a Young's modulus of  $\approx 1.2$  GPa. Notably, the results of nanomechanical testing of hydrated collagen microfibril are in good agreement with available experimental results obtained for the small strain regime based on various techniques such as X-ray diffraction,<sup>29</sup> atomic force microscopy (AFM),<sup>9,27</sup> and the use of microelectro-mechanical

systems (MEMS).<sup>26,28,51</sup> Figure 4b–d and Table 1 present a systematic comparison with a broad range of experimental data based on different techniques. It is noted that for the larger-strain regime there exists less experimental information and available results tend to be more scattered. For example, recent work<sup>28</sup> showed a relatively large variability of collagen fibril behaviors at large deformation, which suggested either strain-hardening or strain-softening depending on the fibril investigated.

A direct comparison of the mechanical properties of single collagen molecules versus that of collagen microfibrils suggests that the mechanical properties are strongly scale dependent. Specifically, we find a severe change of the modulus when comparing a single collagen molecule to a collagen fibril, as shown in Figure 4b and Table 1. A direct numerical comparison suggests a factor of 10–20 difference in the Young's modulus from several gigapascals for a single molecule to a few hundred megapascals for collagen microfibrils, presenting a striking change of mechanical properties at different hierarchical levels. This finding agrees well with experimental data as is confirmed in Table 1.

We now examine the mechanical properties of dehydrated collagen fibrils to test the effect of water solvent on the collagen mechanical properties at the fibril level, which allows us to explore an effect that had earlier been investigated in experimental AFM studies.<sup>27</sup> Our simulation results suggest that dehydrated collagen microfibrils show an almost perfect linear elastic behavior, albeit with a much greater Young's modulus of

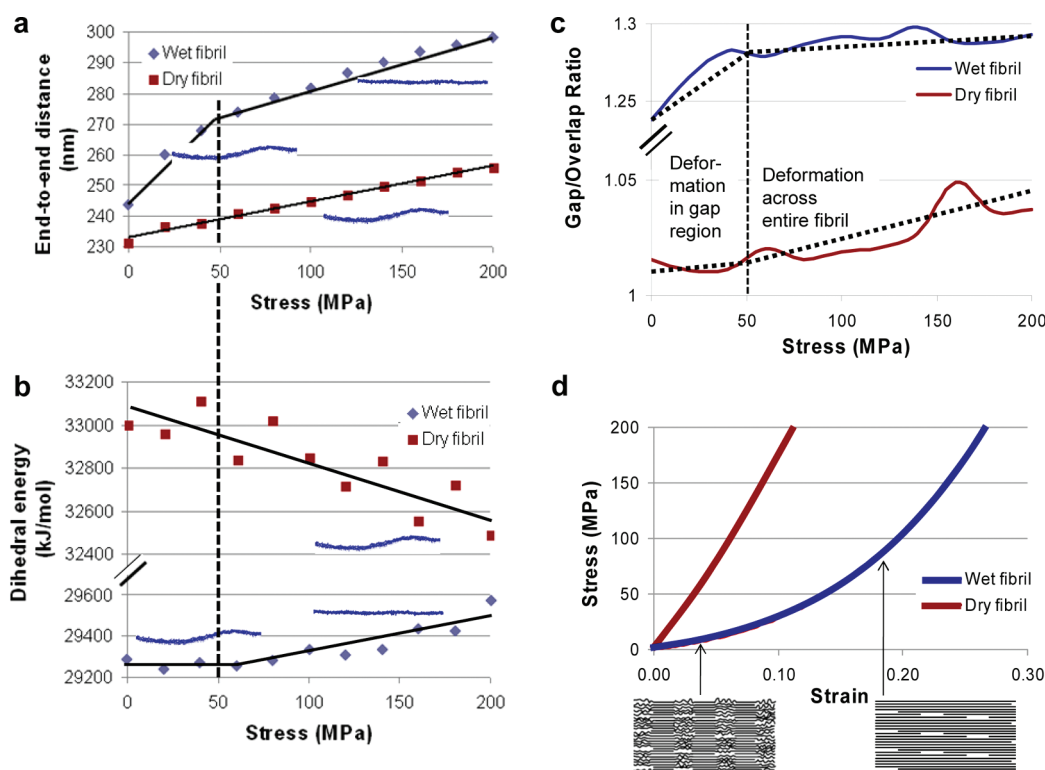


**Figure 5.** Molecular deformation mechanisms during stretching for hydrated and dehydrated collagen microfibril. The two regimes observed in the hydrated microfibril stress–strain curve (showing a larger modulus for strains in excess of 10%, corresponding to an applied stress of  $\approx 50$  MPa) can be explained by analyzing the behavior of single molecules during microfibril stretching. At small deformation, the collagen molecule end-to-end distance increases linearly until the fibril stress reaches  $\approx 50$  MPa. Around this point, the collagen reaches its contour length. Beyond this point, the molecular end-to-end distance still increases but the slope of curve is distinctly smaller (blue, panel a). This is due to the fact that below  $\approx 10\%$  strain the collagen molecule is straightened within the microfibril, while beyond this point the molecule is actually stretched, resulting in a larger resistance of the whole microfibril. The analysis of the dihedral energy of the systems shown in panel b confirms this observation, showing that for stress larger than 50 MPa the dihedral energy increase and thus that the molecule is deformed (blue, panel b). The molecular straightening is concentrated in the gap regions as shown by the increases in the gap/overlap ratio in the low-strain regime (blue, panel c). This suggests a microfibril deformation mechanism in which mechanical load initially straightens collagen molecules, particularly kinks formed in the gap regions, leading to an increase in the gap-to-overlap ratio. For larger loads, collagen triple helices undergo stretching resulting in larger microfibril stiffness (panel d). (Schematics of fibrils adapted from Fratzl et al.<sup>30</sup> and reprinted with permission from Elsevier). In the dehydrated microfibril, the molecular end-to-end distance (red, panel a) increases linearly in the stress range analyzed, while the dihedral energy decreases (red, panel b). This suggests that in the dehydrated microfibril the deformation mechanism initially involves primarily the straightening of the collagen molecules and not stretching of the molecules itself (this is confirmed by the observation that the end-to-end distance at 200 MPa stress is 260 nm, much shorter than the collagen molecules' contour length). The analysis of the gap/overlap ratio (red, panel c) shows that the deformation is initially distributed in both the gap and overlap regions (since the ratio remains constant), and deformation affects the gap region only for larger stresses as shown by the increase in the gap-to-overlap ratio.

$\approx 1.8$  GPa (approaching  $\approx 2.25$  GPa for larger strains), or a striking factor of 6.75 larger than the modulus of hydrated collagen microfibril. Notably, a similar ratio of the moduli in dehydrated versus hydrated states has been observed in experiment<sup>27</sup> where a modulus ratio of 9 between the dehydrated versus hydrated states of the has been identified (see Table 1). These findings point to the great importance of water at the nanoscale for the mechanical properties of collagen microfibrils.

Our atomistic model enables us to observe atomistic and molecular deformation mechanisms not directly accessible to experimental techniques, and thereby to explain the molecular origin of mechanical properties at different hierarchical levels, magnitudes of strain, and under different solvent conditions. We first investigate the molecular mechanisms during fibril stretching, and our studies are specifically aimed at elucidating the mechanisms behind the two regimes observed in the stress–strain curve (Figure 4a) and the changed mechanical properties in hydrated and dehydrated states. For the hydrated case, the

small deformation the collagen molecules' end-to-end distance increases linearly until the microfibril strain reaches 10% (corresponding to  $\approx 50$  MPa stress), the strain at which the microfibril stiffness increases drastically. Beyond this point the molecular end-to-end still continues to increase but the slope of curve is significantly lower (Figure 5a). This can be explained by the fact that below 10% strain the collagen molecule is straightened within the microfibril and thereby loses its kinked arrangement, while beyond 10% strain the molecule itself is being stretched, resulting in a larger mechanical resistance to deformation. The monitoring of the dihedral energy of the systems confirms this hypothesis and shows that for strains larger than 10% the dihedral energy increases, which directly shows that the molecule is being deformed (Figure 5b).

The increase in the gap to overlap ratio in the small-strain regime (Figure 5c) suggests that the initial straightening is concentrated in the gap regions where the molecular packing density is lower and molecules are less organized with more



molecular-scale kinks. Our model thereby directly confirms a suggestion made by Fratzl et al.<sup>3,17</sup> (Figure 5d). However, we note that the straightening of collagen molecules is not limited to the gap regions as collagen molecules in the microfibril feature a kinked geometry throughout the entire structure, which is successively lost during deformation. Once the entire capacity to molecular straightening is exhausted and all collagen molecules assume a straight configuration oriented in the direction of the pulling axis, collagen molecules themselves undergo stretching, leading to a greatly increased tangent microfibril stiffness at strains in excess of 10%. The combination of these two mechanisms, molecular straightening and molecular stretching, effectively lead to an increase of the *D*-period, in direct agreement with experimental results.<sup>52</sup> Other mechanisms, such as molecular sliding may take place at larger strains in excess of 30% as described in earlier studies of the deformation mechanisms.<sup>29,30</sup> Conversely, for the dehydrated collagen microfibril the deformation mechanisms in the investigated stress range involves primarily the straightening of densely packed collagen molecules with little stretching of the collagen molecule itself. This is shown by the increasing molecular end-to-end distance (Figure 5a), which increases linearly, and by the dihedral energy (Figure 5b), which does not increase with the strain. The analysis of the gap-to-overlap ratio (Figure 5c) further shows that deformation is initially equally distributed in both the gap and overlap regions (where the ratio remains constant) and that for larger stresses deformation increasingly affects the gap region (shown by the increase in the gap-to-overlap ratio).

**3. Conclusion.** We have achieved the development of the first experimentally validated all-atom collagen microfibril model with full-length molecules and the explicit simulation of all water molecules with all chemical details. Our model captures all major structural features of collagen microfibrils such as the quasi-hexagonal molecular packing, the *D*-banding periodicity (Figure 2), the distribution of dihedral angles (Figure 3) and most importantly, the very broad range of mechanical behavior at different hierarchical levels and different levels of mechanical deformation (Figure 4 and Table 1). The most important outcome of our study is that deformation of collagen microfibrils is mediated through mechanisms that operate at different hierarchical levels, involving straightening of disordered and helically twisted molecules at small strains, first in the gap regions and then in the entire fibril, followed by axial stretching of molecules, and eventual molecular uncoiling (Figures 4 and 5). Our work has shown that single collagen molecules alone are not capable of providing this broad range of mechanical functionality. Rather, the existence of an array of deformation mechanisms, derived from the hierarchical makeup of the material, is critical to the material's ability to confer key mechanical properties, specifically large extensibility, strain hardening and toughness, despite the inherent limitation that confines the construction of collagenous materials to the use of relatively few amino acids. The paradigm discovered through this analysis exemplifies how functional diversity is achieved through the reliance of structural variation of few and simple building blocks at distinct length-scales (Figure 1), rather than through a great diversity of building blocks. Key architectural features of this material include the formation of a triple helix, a twisted structure of collagen molecules, and a staggered assembly of collagen molecules in fibrils. To highlight the variation of Young's modulus and bending rigidity for a variety of biological and synthetic fibers we present a comparative analysis as shown in Figure 6. This

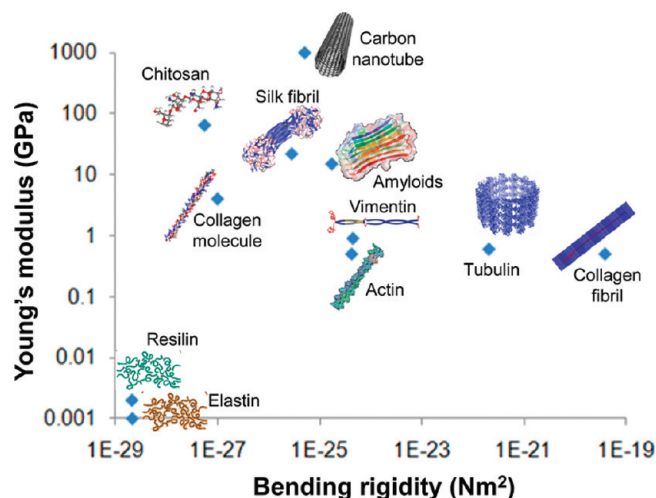


**Figure 6.** Mechanical properties of materials at the nanoscale, comparing both biological and synthetic materials. Biological fibrils and fibers present a vast range of mechanical properties in terms of Young's modulus and bending rigidity.<sup>69–73</sup> However, most of the protein materials feature Young's moduli in the range of 100 MPa to 10 GPa, well below the stiffness of many nanostructured material such as carbon nanotubes. On the other hand, bending rigidity shows a much greater variability. Collagen microfibrils and fibrils present a significantly enhanced bending rigidity with only a relatively small decrease in the Young's modulus compared to a single molecule, showing a greatly effective fibril packing. The analysis shows that collagen fibrils provide a significant bending rigidity at relatively high Young's modulus.

analysis demonstrates that collagen fibrils provide a significant bending rigidity at relatively high Young's modulus.

The observed deformation mechanisms at distinct hierarchical levels explain the striking difference of the Young's modulus of collagen microfibril compared with that of single molecules, which is typically found in the range of  $4.8 \pm 2$  GPa or  $\approx 10$ – $20$  times greater than that of a collagen microfibril. This resolves a long-standing issue in collagen mechanics that has thus far prevented the consolidation of experimental findings with earlier computational results<sup>41,45,46</sup> and demonstrates the importance of geometry and scale of observation in defining mechanical properties of protein materials in general.<sup>17,53–55</sup> Our findings specifically show that the properties of collagen tissues are strongly dependent on the hierarchical level, deformation state (i.e., strain) and hydration level (water content) considered. This suggests that many conventional continuum models of collagen tissues may not be adequate to describe the complex scale-dependent and nonlinear mechanical properties. This has implications for the design of scaffolding materials based on simple polymers, which must include a consideration of the particular nonlinear and scale dependent mechanical properties of matrix materials rather than focusing on the small-deformation bulk modulus alone. Future work could be integrated with recent studies on the effect of hierarchical bonelike materials and provide a computational validation for predictions made about the role of different hierarchies.<sup>55,56</sup>

Another key impact of the experimentally validated molecular model of collagen microfibril mechanics reported here is that it provides a basis to investigate collagenous tissues at the fibril scale and larger. Indeed, with our model it is now possible to assess from a bottom-up perspective how changes at the biochemical and atomistic level (such as amino acid mutations,

cross-link patterns or density, and other molecular defects) affect the structural and mechanical properties at the mesoscale, microscale, and macroscale. This, together with the study of the interaction of collagen fibrils with other biomolecules (e.g., proteoglycans), will provide critical details for the understanding of structure–property relationships in the broader class of collagen tissues. Challenges remain with respect to the greater level of disorder that is expected to be found in collagen fibrils, as outlined in ref 57 and how these structural imperfections, defects, and flaws will influence the mechanical properties. Mechanical models of hierarchical materials and structures suggested that mechanisms exist that mitigate the effects of these defects through flaw-tolerance mechanisms.<sup>58–60</sup> The good agreement between our simulations of perfect microfibrils with experimental results of ones that contain defects may suggest that perhaps an inherent mechanism of flaw-tolerance exists in these structures.

Our model represents a collagen “microfibril”, whereas larger-scale collagen fibrils may feature additional interfaces and disorder between them that could affect the mechanical properties. The construction of such a full collagen fibril mechanics model could be addressed in future work. However, computational challenges associated with such modeling are daunting as the construction of such a model would involve billions of atoms for protein and solvent, a size that is currently out of reach for protein simulations.

A quantitative understanding of elastic moduli at varied scales and deformation states is important in the context of mechanical properties of collagen tissues for cell culture. It has been shown that a cell's microenvironment is important in stem cell lineage specification, where soft matrices that resemble brain tissue-like moduli are neurogenic, stiffer matrices that mimic muscle are myogenic, and rigid matrices that mimic bone prove to be osteogenic.<sup>61</sup> Cells act at the micrometer scale, the scale of collagen microfibrils, fibrils, and fibers, and their behavior is likely directed by the complex hierarchical structure of their surrounding environment. However, current biomaterials used for scaffolding do not present a hierarchical structure such as that found in natural ECM materials, which may affect the cell behavior and differentiation. Indeed, a clear understanding of collagen's scale and strain dependent stiffness may help in designing biomaterials with appropriate mechanical characteristics and thus addresses an immediate need for optimized matrix elasticity to foster differentiation and enhanced performance for regenerative medicine applications based on stem cell therapies such as cardiomyoplasty, muscular dystrophy, and neuroplasty.<sup>62,63</sup>

Our model of collagen microfibril mechanics is based on X-ray diffraction results and is limited by the range of molecular conformation changes that can be observed at a molecular dynamics time-scale. For example, even though the mechanical analysis of the modulus of dehydrated collagen microfibril agrees well with experimental findings (with similar Young's modulus values as shown in Table 1), the Ramachandran analysis suggests a heightened level of disorder in the system, perhaps indicative of molecular unfolding. Drastic changes in the molecular architecture associated with such mechanisms could be explored via the use of advanced computational methods, such as replica exchange molecular dynamics and may be combined with experimental efforts.<sup>57</sup> The computational challenges associated with these methods are, however, enormous. A limitation of the collagen microfibril mechanics model is that it is based on the periodic repetition of a crystallographic unit cell, necessitated by

the significant computational cost associated with simulating this large molecular structure. The periodic model also implies that no cross-links between molecules are considered and that sliding between triple helical collagen molecules is not taken into account. Despite these limitations, as confirmed in Table 1, the model properly captures the mechanical behavior seen in experiments, likely because the above listed constraints do not affect the behavior at relatively small deformation below 20–30% strain. Indeed, the effects of cross-links between molecules and intermolecular sliding have been shown to dominate the properties primarily at larger deformation.<sup>64</sup> A microfibril model that explicitly considers multiple molecules poses no fundamental challenge; however, it would be rather challenging from a computational point of view. As appropriate computational resources become available, however, development of such models should be straightforward by extending the work reported here.

**4. Materials and Methods.** Existing collagen microfibril and fibril models represent the supramolecular arrangement in collagenous tissues in a simplified way, using a two-dimensional lattice of mesoscopic beads<sup>45,46</sup> or extremely short collagen peptides.<sup>36–41</sup> These models do not account for the biochemical details and are much smaller than the typical length-scales of collagen molecules found in collagen microfibrils and fibrils. The reason for these approximations is that up until now crystallographic details (and in particular a full-atomistic geometry) of the collagen molecule have been obtained only for short collagen-like peptides with lengths below  $\approx 10$  nm.<sup>32–34</sup> The method applied here overcomes these limitations and enables us to develop a full atomistic model of the mechanics of collagen microfibrils.

*Homology Modeling.* The structural model of the collagen microfibril is generated starting from the in situ structure of full length collagen type I molecule<sup>8</sup> (Protein Data Bank identification code 3HR2). This structure, obtained by employing conventional crystallographic techniques in X-ray fiber diffraction experiments, resolved for the first time the specific three-dimensional arrangement of collagen molecules in naturally occurring fibrils, including the N- and C-telopeptides. Since the structure reported in ref 8 includes only backbone  $\alpha$ -carbons and the primary sequence of *Rattus norvegicus*, we used homology modeling to obtain a full-atom structure with the human collagen sequence. The sequence of the human type I collagen is obtained from PubMed (entry number NP\_000079 for  $\alpha 1(I)$  chain and NP\_000080 for the  $\alpha 2(I)$  chain). The 3HR2 structure and the human collagen type I sequence are aligned, and ten homology models are built and scored by the discrete optimized protein energy (DOPE) using the Modeler program (version 9.6).<sup>65</sup> The structure with the lowest DOPE value is chosen for building the collagen microfibril model.

*Fibril Model Generation.* The collagen supramolecular model (microfibril) is generated using the information on the naturally occurring crystallographic unit cell reported in ref 8, and in the associated 3HR2 structure ( $a \approx 40.0$  Å,  $b \approx 27.0$  Å,  $c \approx 678$  Å,  $\alpha \approx 89.2^\circ$ ,  $\beta \approx 94.6^\circ$ ,  $\gamma \approx 105.6^\circ$ ). The molecular packing topology obtained by the periodic repetition of the unit cell lead to quasi-hexagonally packed collagen molecules which interdigitates with neighboring molecules to form a supertwisted right-handed microfibril and to the well-known D-banding periodicity seen in AFM images of collagen fibrils. The fibril model is solvated using the solvate plug in of GROMACS by adding



SPC water molecules. Since the molecule at physiological pH includes a net charge (positive net charge +34), counterions ( $\text{Cl}^-$ ) are added in order to keep the system neutral. The final solvated all-atom system contains  $\approx 57\,000$  atoms, including  $\sim 32\,000$  water atoms. The first step of energy minimization is performed by a steepest descent algorithm using the GROMACS 4.0 code<sup>66</sup> and the GROMOS 43a1 force field, which includes parameters for hydroxyproline amino acid (HYP) found in collagen. This force field has been widely validated for a variety of biochemical models of proteins including collagen.<sup>40,41</sup>

**All-Atom Equilibration.** Full atomistic simulations are carried out using the GROMACS 4.0 code.<sup>66</sup> Rigid bonds are used to constrain covalent bond lengths, thus allowing an integration time step of 2 fs. Nonbonding interactions are computed using a cutoff for the neighbor list at 1.35 nm with a switching function between 1.0 and 1.2 nm for Van Der Waals interactions, while the particle-mesh Ewald summation (PME) method is applied to describe electrostatic interactions. The fibril model is equilibrated through 8.5 ns NPT molecular dynamics simulations at a temperature of 310 K (37 °C) and with 1 bar pressure. We use a velocity-rescaling thermostat with 1 ps coupling constant and a Berendsen barostat with 1 ps time constant. We ensure structural convergence through a root mean square deviation (rmsd) analysis, where convergence is confirmed when the slope of the rmsd with respect to time approaches zero for all levels of applied stress.

**In Silico Mechanical Testing.** To assess the mechanical properties of the hydrated and dehydrated atomistic microfibril models, we perform molecular dynamics simulations with increasing constant mechanical stress in tension along the fibril axis while maintaining the pressure on the other axes constant at 1 bar (using a Berendsen barostat and 1 ps coupling constant). Although the  $c$  axis (the long axis) of the periodic unit cell is not perfectly aligned parallel with the microfibril direction (by an angle mismatch of about 1°), the effect on the mechanical properties (the focus of this study) is very small since the mechanical load is reasonably well aligned with the overall direction of the microfibril. The mechanical loading implemented here reflects the setup that is also used for mechanical testing in experimental studies. The applied stresses are in the range from 0 to 200 MPa, applied during 20 ns molecular dynamics simulation for each load applied. We find that equilibrium of the molecular structure is reliably reached within 10–15 ns of molecular dynamics simulation, depending on the extent of the deformation. Thus we use the last 5 ns of molecular dynamics simulation for the mechanical analysis after the system has fully converged. To ensure that equilibrium is obtained, we monitor pressure equilibrium, protein rmsd, and confirm that the size of the simulation cell reaches a steady value. The strain  $\varepsilon(\sigma)$  is calculated as follows

$$\varepsilon(\sigma) = \frac{L(\sigma) - L_0}{L_0} \quad (1)$$

where  $L(\sigma)$  is the equilibrium cell length along the microfibril axis when a strain  $\sigma$  is applied, while  $L_0$  is the equilibrium cell length along the fibril axis for  $\sigma = 0$ . From the fibril strains  $\varepsilon(\sigma)$  resulting from each applied stress  $\sigma$ , we obtain the stress–strain behavior as plotted in Figure 4.

**Computational Method and Cost.** Because of the size of the model, all-atom simulations of the collagen microfibril with explicit solvent are computationally very intense. The fully

solvated (full-atomistic model contains  $\approx 57\,000$  atoms ( $\approx 25\,000$  in the dehydrated [dry] model), requiring about 6 h per nanosecond on 32 CPUs on a parallel machine. Since phenomena involving the molecular (and supramolecular) scale are often in the range of several nanoseconds or even microseconds, molecular dynamics simulations of the full-atomistic collagen fibril are at the limit of current computational capabilities.

## AUTHOR INFORMATION

### Corresponding Author

\*E-mail: mbuehler@MIT.EDU.

### Notes

The authors declare no competing interests of any sort.

## ACKNOWLEDGMENT

The authors thank Joseph Orgel (Pritzker Institute of Biomedical Science and Engineering at the Illinois Institute of Technology and Argonne National Lab, U.S.A.), Sandra Shefelbine (Department of Bioengineering at Imperial College, London, U.K.), John Currey (University of York, U.K.) and Steve Cowin (City College New York, U.S.A.) for their helpful suggestions during the preparation of this manuscript. This research was supported by NSF (Grant CMMI-0642545), ONR (Grant N000141010562), by the MIT-Italy program “Progetto Rocca” and by Politecnico di Milano (Grant “5 per mille junior 2009”). High-performance computing resources have been provided by Regione Lombardia and CILEA Consortium through a LISA Initiative (Laboratory for Interdisciplinary Advanced Simulation) 2010 grant and by CINECA under the ISCRA initiative as well as NSF TeraGrid.

## REFERENCES

- (1) Kadler, K. E.; Baldock, C.; Bella, J.; Boot-Handford, R. P. *J. Cell Sci.* **2007**, *120* (12), 1955–1958.
- (2) Cowin, S. C.; Doty, S. B. *Tissue Mechanics*; Springer: New York, 2007.
- (3) Fratzl, P. *Collagen: Structure and Mechanics*. Springer: New York, 2008.
- (4) Fraser, R. D.; MacRae, T. P.; Miller, A.; Suzuki, E. *J. Mol. Biol.* **1983**, *167* (2), 497–521.
- (5) Hulmes, D. J. S.; Wess, T. J.; Prockop, D. J.; Fratzl, P. *Biophys. J.* **1995**, *68* (5), 1661–1670.
- (6) Orgel, J. P. R. O.; Miller, A.; Irving, T. C.; Fischetti, R. F.; Hammersley, A. P.; Wess, T. J. *Structure* **2001**, *9*, 1061–1069.
- (7) Currey, J. D. *Bones: Structure and Mechanics*; Princeton University Press: Princeton, NJ, 2002.
- (8) Orgel, J. P. R. O.; Irving, T. C.; Miller, A.; Wess, T. J. *Proc. Natl. Acad. Sci. U.S.A.* **2006**, *103* (24), 9001–9005.
- (9) Aladin, D. M.; Cheung, K. M.; Ngan, A. H.; Chan, D.; Leung, V. Y.; Lim, C. T.; Luk, K. D.; Lu, W. W. *J. Orthop. Res.* **2010**, *28* (4), 497–502.
- (10) Petruska, J. A.; Hodge, A. J. *Proc. Natl. Acad. Sci. U.S.A.* **1964**, *51* (5), 871.
- (11) Moeller, H. D.; Bosch, U.; Decker, B. *J. Anat.* **1995**, *187*, 161–167.
- (12) Weiner, S.; Wagner, H. D. *Ann. Rev. Mater. Sci.* **1998**, *28*, 271–298.
- (13) Brianza, S. Z. M.; D'Amelio, P.; Pugno, N.; Delise, M.; Bignardi, C.; Isaia, G. *Bone* **2007**, *40* (6), 1635–1642.
- (14) Gupta, H. S.; Seto, J.; Wagermaier, W.; Zaslansky, P.; Boesek, P.; Fratzl, P. *Proc. Natl. Acad. Sci. U.S.A.* **2006**, *103*, 17741–17746.
- (15) Gupta, H. S.; Wagermaier, W.; Zickler, G. A.; Aroush, D. R. B.; Funari, S. S.; Roschger, P.; Wagner, H. D.; Fratzl, P. *Nano Lett.* **2005**, *5* (10), 2108–2111.

- (16) Gupta, H. S.; Messmer, P.; Roschger, P.; Bernstorff, S.; Klaushofer, K.; Fratzl, P. *Phys. Rev. Lett.* **2004**, 93 (15), No. 158101.
- (17) Fratzl, P.; Weinkamer, R. *Prog. Mater. Sci.* **2007**, 52, 1263–1334.
- (18) Camacho, N. P.; Hou, L.; Toledano, T. R.; Ilg, W. A.; Brayton, C. F.; Raggio, C. L.; Root, L.; Boskey, A. L. *J. Bone Miner. Res.* **1999**, 14 (2), 264–272.
- (19) Fratzl, P.; Gupta, H. S.; Paschalis, E. P.; Roschger, P. *J. Mater. Chem.* **2004**, 14 (14), 2115–2123.
- (20) Pugno, N. M. *Nanotechnology* **2006**, 17 (21), 5480–5484.
- (21) Carpinteri, A.; Pugno, N. M. *Int. J. Fract.* **2008**, 150 (1–2), 221–226.
- (22) Cusack, S.; Miller, A. *J. Mol. Biol.* **1979**, 135 (1), 39–51.
- (23) Sun, Y.; Luo, Z.; Fertala, A.; An, K. *Biochem. Biophys. Res. Commun.* **2002**, 295 (2), 382–386.
- (24) Bozec, L.; Horton, M. *Biophys. J.* **2005**, 88 (6), 4223–4231.
- (25) Buehler, M. J.; Wong, S. Y. *Biophys. J.* **2007**, 93 (1), 37–43.
- (26) Eppell, S. J.; Smith, B. N.; Kahn, H.; Ballarini, R. *J. R. Soc. Interface* **2006**, 3 (6), 117–121.
- (27) van der Rijt, J. A. J.; van der Werf, K. O.; Bennink, M. L.; Dijkstra, P. J.; Feijen, J. *Macromol. Biosci.* **2006**, 6 (9), 697–702.
- (28) Shen, Z. L.; Dodge, M. R.; Kahn, H.; Ballarini, R.; Eppell, S. J. *Biophys. J.* **2008**, 95 (8), 3956–3963.
- (29) Sasaki, N.; Odajima, S. *J. Biomech.* **1996**, 29 (9), 1131–1136.
- (30) Fratzl, P.; Misof, K.; Zizak, I.; Rapp, G.; Amenitsch, H.; Bernstorff, S. *J. Struct. Biol.* **1998**, 122 (1–2), 119–122.
- (31) Fratzl, P.; Burgert, I.; Gupta, H. S. *Phys. Chem. Chem. Phys.* **2004**, 2004, 5575–5579.
- (32) Beck, K.; Chan, V. C.; Shenoy, N.; Kirkpatrick, A.; Ramshaw, J. A. M.; Brodsky, B. *Proc. Natl. Acad. Sci. U.S.A.* **2000**, 97 (8), 4273–4278.
- (33) Bella, J.; Eaton, M.; Brodsky, B.; Berman, H. M. *Science* **1994**, 266 (5182), 75–81.
- (34) Xu, Y.; Persikov, A.; Jordan, J.; Brodsky, B. *Biophys. J.* **2000**, 78 (1), 425A–425A.
- (35) Redaelli, A.; Vesentini, S.; Soncini, M.; Vena, P.; Mantero, S.; Montevercchi, F. M. *J. Biomech.* **2003**, 36 (10), 1555–1569.
- (36) Mogilner, I. G.; Ruderman, G.; Grigera, J. R. *J. Mol. Graphics Modell.* **2002**, 21 (3), 209–213.
- (37) Lorenzo, A. C.; Caffarena, E. R. *J. Biomech.* **2005**, 38 (7), 1527–1533.
- (38) Buehler, M. J. *J. Mater. Res.* **2006**, 21 (8), 1947–1961.
- (39) Bhowmik, R.; Katti, K. S.; Katti, D. R. *J. Mater. Sci.* **2007**, 42 (21), 8795–8803.
- (40) Gautieri, A.; Buehler, M. J.; Redaelli, A. *J. Mech. Behav. Biomed. Mater.* **2009**, 2 (2), 130–137.
- (41) Gautieri, A.; Uzel, S.; Vesentini, S.; Redaelli, A.; Buehler, M. J. *Biophys. J.* **2009**, 97 (3), 857–865.
- (42) Hofmann, H.; Voss, T.; Kuhn, K.; Engel, J. *J. Mol. Biol.* **1984**, 172 (3), 325–343.
- (43) Sasaki, N.; Odajima, S. *J. Biomech.* **1996**, 29 (5), 655–658.
- (44) Harley, R.; James, D.; Miller, A.; White, J. W. *Nature* **1977**, 267 (5608), 285–287.
- (45) Buehler, M. J. *Proc. Natl. Acad. Sci. U.S.A.* **2006**, 103 (33), 12285–12290.
- (46) Buehler, M. J. *J. Mech. Behav. Biomed. Mater.* **2008**, 1 (1), 59–67.
- (47) Rauch, F.; Glorieux, F. H. *Lancet* **2004**, 363, 1377–85.
- (48) Holmes, D. F.; Gilpin, C. J.; Baldock, C.; Ziese, U.; Koster, A. J.; Kadler, K. E. *Proc. Natl. Acad. Sci. U.S.A.* **2001**, 98 (13), 7307–7312.
- (49) Chapman, E. W.; Rodriguez, F. *Polym. Eng. Sci.* **1977**, 17 (5), 282–286.
- (50) Brodsky, B.; Ramshaw, J. A. M. *Matrix Biol.* **1997**, 15 (8–9), 545–554.
- (51) Espinosa, H. D.; Zhu, Y.; Moldovan, N. *J. Microelectromech. Syst.* **2007**, 16 (5), 1219–1231.
- (52) Kukreti, U.; Belkoff, S. M. *J. Biomech.* **2000**, 33 (12), 1569–1574.
- (53) Carpinteri, A.; Pugno, N. *Nat. Mater.* **2005**, 4 (6), 421–3.
- (54) Pugno, N. M. *Acta Mater.* **2007**, 55 (6), 1947–1953.
- (55) Zhang, Z.; Zhang, Y. W.; Gao, H. *Proc. R. Soc. London, Ser. B* **2010**; DOI: 10.1098/rspb.2010.1093.
- (56) Pugno, N. M.; Carpinteri, A. *Philos. Mag. Lett.* **2008**, 88 (6), 397–405.
- (57) Perumal, S.; Antipova, O.; Orgel, J. P. *Proc. Natl. Acad. Sci. U.S.A.* **2008**, 105 (8), 2824–9.
- (58) Pugno, N. M.; Bosia, F.; Carpinteri, A. *Small* **2008**, 4 (8), 1044–1052.
- (59) Pugno, N. M. *Appl. Phys. Lett.* **2007**, 90 (4), No. 043106.
- (60) Gao, H.; Ji, B.; Jäger, I. L.; Arzt, E.; Fratzl, P. *Proc. Natl. Acad. Sci. U.S.A.* **2003**, 100 (10), 5597–5600.
- (61) Engler, A. J.; Sen, S.; Sweeney, H. L.; Discher, D. E. *Cell* **2006**, 126 (4), 677–689.
- (62) Yow, S. Z.; Quek, C. H.; Yim, E. K.; Lim, C. T.; Leong, K. W. *Biomaterials* **2009**, 30 (6), 1133–42.
- (63) LeDuc, P. R.; Robinson, D. N. *Adv. Mater.* **2007**, 19, 3761–3770.
- (64) Uzel, S.; Buehler, M. J. *J. Mech. Behav. Biomed. Mater.* **2010**; DOI: 10.1016/j.jmbbm.2010.07.003.
- (65) Fiser, A.; Sali, A. *Macromol. Crystallogr., Part D* **2003**, 374, 461.
- (66) Berendsen, H. J. C.; Vanderspoel, D.; Vandrunen, R. *Comput. Phys. Commun.* **1995**, 91 (1–3), 43–56.
- (67) Vesentini, S.; Fittie, C. F. C.; Montevercchi, F. M.; Redaelli, A. *Biomech. Model. Mechanobiol.* **2005**, 3 (4), 224–234.
- (68) Gautieri, A.; Russo, A.; Vesentini, S.; Redaelli, A.; Buehler, M. J. *J. Chem. Theory Comput.* **2010**, 6 (4), 1210–1218.
- (69) Smith, J. F.; Knowles, T. P. J.; Dobson, C. M.; MacPhee, C. E.; Welland, M. E. *Proc. Natl. Acad. Sci. U.S.A.* **2006**, 103 (43), 15806–15811.
- (70) Nishino, T.; Matsui, R.; Nakamae, K. *J. Polym. Sci., Part B: Polym. Phys.* **1999**, 37 (11), 1191–1196.
- (71) Gosline, J. M.; Guerette, P. A.; Ortlepp, C. S.; Savage, K. N. *J. Exp. Biol.* **1999**, 202 (23), 3295–3303.
- (72) Ketten, S.; Xu, Z. P.; Ihle, B.; Buehler, M. J. *Nat. Mater.* **2010**, 9 (4), 359–367.
- (73) Deriu, M. A.; Enemark, S.; Soncini, M.; Montevercchi, F. M.; Redaelli, A. *J. Mater. Sci.* **2007**, 42 (21), 8864–8872.

#### ■ NOTE ADDED AFTER ASAP PUBLICATION

Due to a production error, this paper published January 5, 2011 with an incorrect abstract image. The correct version published January 7, 2011.